PHYSICAL REVIEW B VOLUME 31, NUMBER 6 15 MARCH 1985

Electronic coherence length following pulsed-laser annealing of Cu(001)

S. D. Kevan
AT&T Bell Laboratories, Murray Hill, New Jersey 07974
(Received 22 August 1984)

High-resolution angle-resolved photoemission experiments are reported which examine the quality of a pulsed-laser-annealed Cu(001) surface. A significant degradation of the electronic coherence length is observed for laser pulse energies above a certain threshold. This is attributed to defect production following melting of the surface layers. In addition, above threshold, the defect density and the electron coherence length are found to be determined primarily by the integrated laser-energy density.

I. INTRODUCTION

High-energy pulsed lasers are currently finding novel applications in surface and near-surface materials processing.[1–10] While the primary motivation for such studies is the fabrication of improved electronic devices, various investigations have demonstrated the utility of pulsed-laser annealing (PLA) in rapid surface cleaning as well as in the production of original surface structures.[3–8] Characterization of the electronic and geometric structures obtained following PLA is thus of considerable practical and fundamental interest. Various surface and bulk probes have been applied with this goal in mind, and one recurring result has arisen:[8–11] Defect densities increase following PLA of both metals and semiconductors. It is important to characterize the effect of these defects on electronic structure.

High-resolution angle-resolved photoemission (ARP) experiments have recently been shown to provide information on the crystalline quality of the surface layers.[12–14] The information derived is complementary to that available from high-resolution low-energy electron diffraction (LEED) studies. This can be seen by considering ARP and LEED experiments performed on a crystalline material containing a random array of point defects or impurities. As long as atoms on either side of a defect are in registry (the defect does not change the long-range order of the substrate), the presence of the defect will not appreciably affect the measured LEED coherence: Beams will remain sharp, albeit with reduced contrast over the background intensity. The situation in ARP is quite different. The initial-state valence electron can scatter off the defect and will have a mean-free-path or coherence length given by[12]

$$\lambda=\Omega_0(c\sigma)^{-1}\,, \tag{1}$$

where c is the concentration of defects, σ is a measure of the energy-dependent scattering cross section, and Ω_0 is the unit-cell volume. The ARP final state will be affected in a similar manner with its own characteristic length. However, the scattering cross section $\sigma(E)$ normally decreases rapidly with energy so that in general the coherence length in ARP is expected to be dominated by the initial-state electronic coherence length. This prediction is supported by the fact that the ARP final state is the time-reversed LEED state and its coherence length will be reflected by that of the LEED experiment. The coherence lengths measured in ARP are typically an order of magnitude smaller than those measured by LEED. Equation (1) is too simple in the general case which contains ill-defined point and line defects, but we may still think of an electronic coherence length for a particular surface preparation.

The experiments reported here examine the quality of a pulsed-laser-annealed Cu(001) surface under ultrahigh-vacuum conditions. The results demonstrate a novel application of the ARP technique as well as a significant degradation of coherence length following PLA for pulse energies above the melting threshold. With reference to previous investigations, this degradation is attributed to defect production. As such, these results constitute a systematic application of ARP in determining surface quality following a novel cleaning-preparation procedure.

The structure of this paper is as follows. Section II discusses a simple yet general treatment of the effect of static disorder on observed ARP peak widths and demonstrates the optimal experimental parameters in such investigations. Section III describes the experimental procedures used, while Sec. IV shows experimental results on laser-annealed Cu(001) and interprets them within the framework of Sec. II. Finally, Sec. V summarizes the results and speculates on the future of such experiments.

II. STATIC DISORDER IN ARP

The treatment starts by considering the photoemission intensity into a small angular cone $d\Omega$:[15,16]

$$\frac{dI}{d\Omega}\sim|\langle\psi(\mathbf{k}_i)|\hat{O}|\psi(\mathbf{k}_f)\rangle|^2\,, \tag{2}$$

where $\psi(\mathbf{k}_i)$ and $\psi(\mathbf{k}_f)$ are the initial- and final-state wave functions for the imperfect crystal and $\hat{O}$ is the interaction operator of the photon field. The momenta $\mathbf{k}_i$ and $\mathbf{k}_f$ label these states in the sense discussed below but are not good quantum numbers derived from the perfect lattice. If the disorder is not severe, we can expand in terms of the Bloch wave functions of the perfect crystal $\phi(\mathbf{k})$:

$$\psi(\mathbf{k}_i)=\sum_{\Delta\mathbf{k}}\alpha(\mathbf{k}_i+\Delta\mathbf{k})\phi(\mathbf{k}_i+\Delta\mathbf{k}) \tag{3}$$

with a similar equation for $\psi(\mathbf{k}_f)$. The coefficients $\alpha(\mathbf{k})$ will be significant in magnitude only near $\mathbf{k}_i$; and $\Delta\mathbf{k}_0$, the full width at half maximum of the distribution $\alpha(\mathbf{k})$, is given approximately by the inverse of the electronic coherence length defined in the Introduction. From the arguments given there this width for the final state will be negligibly small compared to that of the initial state, so that

$$\psi(\mathbf{k}_f)\approx\phi(\mathbf{k}_f) \ . \tag{4}$$

Substituting (3) and (4) into (2), we get

$$\frac{dI}{d\Omega}=\left|\left\langle\sum_{\Delta\mathbf{k}}\alpha(\mathbf{k}_i+\Delta\mathbf{k})\phi(\mathbf{k}_i+\Delta\mathbf{k})\,|\,\hat{O}\,|\,\phi(\mathbf{k}_f)\right\rangle\right|^2$$
$$=\left|\sum_{\Delta\mathbf{k}}\alpha(\mathbf{k}_i+\Delta\mathbf{k})\langle\phi(\mathbf{k}_i+\Delta\mathbf{k}\,|\,\hat{O}\,|\,\phi(\mathbf{k}_f)\rangle\right|^2 . \tag{5}$$

For small $\Delta\mathbf{k}_0$ (minimal disorder), the matrix elements are approximately constant:

$$\langle\phi(\mathbf{k}_i+\Delta\mathbf{k})\,|\,\hat{O}\,|\,\phi(\mathbf{k}_f)\rangle\sim\langle\phi(\mathbf{k}_i)\,|\,\hat{O}\,|\,\phi(\mathbf{k}_f)\rangle$$
$$=M(\mathbf{k}_i,\mathbf{k}_f) \ , \tag{6}$$

and we get

$$\frac{dI}{d\Omega}\sim|\,M(\mathbf{k}_i,\mathbf{k}_f)\,|^2\sum_{\Delta\mathbf{k}}|\,\alpha(\mathbf{k}_i+\Delta\mathbf{k})\,|^2 \ . \tag{7}$$

If we ignore the matrix element for a moment, we see that the sum implies that the defects allow transitions in the vicinity of $\mathbf{k}_i$, weighted by $|\,\alpha(\mathbf{k}_i+\Delta\mathbf{k})\,|^2$. Since $\nabla_k E(\mathbf{k}_i)$ given by the valence-band structure is in general nonzero, this sum implies spectral broadening. In principle, the observed peak width and shape reflect the expansion coefficients. The situation is complicated by momentum broadening allowed by the matrix element, but there should still be a contribution to the observed width due to disorder:

$$\Delta E_1=\nabla_{\mathbf{k}}E(\mathbf{k}_i)\cdot\Delta\mathbf{k}_0 \ . \tag{8}$$

We might hope to extract the electronic coherence length from the observed spectral width.

The finite lifetime of the final-state electron and hole implies intrinsic momentum broadening normal to the surface.[15–17] Note that this broadening is a lifetime effect implying a complex but diagonal energy matrix, while the effect of static disorder forces the energy matrix to be nondiagonal in the perfect-crystal basis set. This lifetime broadening is a well-documented effect and has been given a complete first-order treatment elsewhere.[15] Its Lorentzian contribution to the observed ARP peak width enters through the matrix element $M(\mathbf{k}_i,\mathbf{k}_f)$:

$$\Delta E_0=\frac{\Gamma_h+|\,v_h^\perp/v_e^\perp\,|\,\Gamma_e}{|\,(1-mv_h^{\parallel}\sin^2\theta/\hbar k_{\parallel})-v_h^\perp/v_e^\perp(1-mv_e^{\parallel}\sin^2\theta/\hbar k_{\parallel})\,|} \ . \tag{9}$$

In this equation, $v_h^\perp$ and $v_h^{\parallel}$ are the final-state hole velocities normal and parallel to the surface, respectively, while $v_e^\perp$ and $v_e^{\parallel}$ are those of the photoelectron. Γ_h and Γ_e are the inverse lifetimes of the final-state hole and electron, m is the electron mass, θ is the emission angle, and $k_{\parallel}$ is the momentum parallel to the surface. Equation (7) can thus be viewed as yielding a peak which is the sum of Lorentzian line shapes located at $\mathbf{k}_i+\Delta\mathbf{k}$ weighted by the coefficients $|\,\alpha(\mathbf{k}_i+\Delta k)\,|^2$. The observed width is thus a convolution of a Lorentzian of width given by Eq. (9) with a generally unknown line shape with a width given by Eq. (8). Ideally, to extract information on ΔE_1 and $\Delta\mathbf{k}_0$, we want to operate with ΔE_0 as small as possible while maintaining sensitivity to ΔE_1. The method for limiting ΔE_0 has been discussed elsewhere.[15–17] The contribution from Γ_h is made small by operating near the Fermi energy E_F, while that from Γ_e can be made small by limiting $v_h^\perp$. $v_h^\perp$ is rigorously zero for a two-dimensional state, which implies advantageous use of an intrinsic surface state to extract $\Delta\mathbf{k}_0$. This has been shown to work well for a nominally clean and well-ordered surface.[12–14] In studying the effect of induced defects, however, an intrinsic surface state is not a good choice since the state is often destroyed by small quantities of defects or impurities. An alternative technique is to sample a more resilient three-dimensional bulk state near an appropriate symmetry point where $v_h^\perp$ is zero. One must be careful, however, since if a point is chosen where $v_h^{\parallel}$ is zero as well, the sensitivity to ΔE_1 is minimal from Eq. (8).

The optimal experimental parameters for extracting $\Delta\mathbf{k}_0$ therefore are a bulk feature located near E_F with $v_h^\perp=0$ and $v_h^{\parallel}$ large. A very simple procedure using Fermi-surface data for locating such a feature is available. Figure 1 shows the Fermi surface of copper in the $\Gamma-L-U-X-\Gamma$ plane. The condition that $v_h^\perp=0$ near E_F is equivalent to finding points such that a line of constant $\mathbf{k}_{\parallel}$ is tangent to the Fermi surface, while $v_h^{\parallel}$ is maximized when a line of constant $\mathbf{k}_\perp$ intersects the Fermi surface at 90°. For Cu(001) this occurs at the ends of the "neckties" of the Fermi surface $[\mathbf{k}=(2\pi/a)(1/2,1/2,1]$. This projects onto the $\bar{X}$ point of the surface Brillouin zone. Since in these studies fixed frequency resonance radiation was available, this optimal point was not accessible. The solid circle centered at $\mathbf{k}=(0,0,0)$ corresponds to a free-electron state at $h\nu=16.8$ eV(Ne I radiation). Of the two Fermi-surface intersections, the one labeled B is

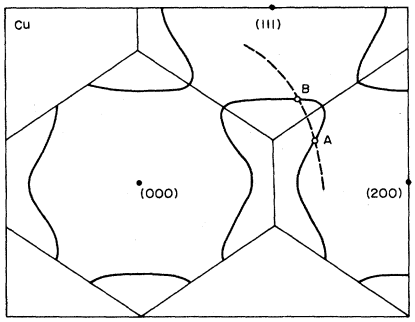

FIG. 1. Fermi surface of copper in the $\Gamma-L-U-X-\Gamma$ plane of the bulk Brillouin zone. The circle centered at the center of the first zone is a free-electron final state at $\sim$17 eV above E_F.

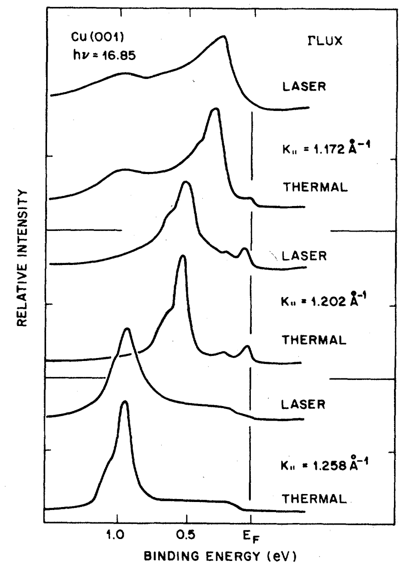

FIG. 2. EDC's for initial states near E_F near the $\overline{X}$ point of Cu(001). The small feature near E_F in the middle pair of EDC's is a surface state. All features are split by the Ne I doublet. In each pair, the lower curve was taken following a thermal anneal, while the upper curves followed a pulsed-laser anneal.

adequate for our purposes: $v_h^{\perp}/v_e^{\perp} \sim 0.01$, $v_h^{\parallel} \sim 8$ eV/Å^{-1}. A complete comparison of these two intersections is given elsewhere.[12]

III. EXPERIMENTAL PROCEDURES

Experiments were performed in a photoemission spectrometer which has been described elsewhere.[18] The energy and angular resolution used in the present studies were 20—25 meV and 0.6°, respectively. At the Ne I photon energy used ($h\nu = 16.85$ eV), this angular resolution yields a momentum resolution of $\Delta k_{\parallel} \sim 0.01$ Å^{-1}. This in effect limits the ultimate resolution of $\Delta \mathbf{k}_0$ from the preceding section. The Cu(001) sample was cleaned by repeated cycles of neon-ion bombardment followed by thermal annealing to 750 K for 5 min. This procedure produced a surface of exceptional crystalline quality; LEED beams typically measured $<1°$ in width. The natural widths were estimated to be substantially less. Impurities were detectable using Auger-electron spectroscopy (AES) implying residual concentrations of <0.01 monolayer. The laser radiation was supplied by a pulsed XeCl excimer laser equipped with an electrode which produced a beam which was spatially uniform to within 10%.[19] Pulse energies were 0—400 mJ and the pulse width was 25—30 nsec. The ultraviolet laser light couples to a polished copper surface significantly better than that of a visible—near-infrared laser.[9] The laser beam was focused through a sapphire window onto a $0.1-\text{cm}^2$ spot on the sample in a fashion which preserved the beam quality. Pulse energies were measured in a relative sense to $\pm 5\%$, but uncertainties in focusing produced an uncertainty of $\pm 25\%$ in absolute energy density at the sample. Since the spectrometer focus is only ~ 0.01 cm^2,[18] rastering of either the laser beam or the sample was not necessary.[9] During PLA, the chamber pressure was stable in the low 10^{-10}-Torr range.

IV. RESULTS AND DISCUSSION

Figure 2 shows three pairs of ARP energy-distribution curves (EDC's) taken from Cu(001) for initial-state momenta near the $\overline{X}$ symmetry point of the two-dimensional Brillouin zone. The larger peak which disperses rapidly with parallel momentum arises from momentum conserving transitions from band 6 of the bulk copper band structure near point B in Fig. 1. For each pair, the bottom curve is taken after a thermal anneal (700 K, 2 min), while the top curve has been taken after a pulsed-laser anneal (50 shots, 1.0 J/cm^2). In each case, the bulk feature broadens significantly after laser annealing. The thermally annealed result is recovered after a mild anneal (600 K, <1 min). This broadening is ascribed to degradation of the surface with the consequent shortening of the electronic coherence length, as described in the following paragraphs.

Other comparisons of the laser- and thermal-annealed surfaces were performed. The LEED patterns were both quite sharp, though that of the laser-annealed surface had an increased background. Measurements of the LEED spot profile at a few scattering energies did not show significant differences between the surfaces. Contamination of both surfaces was below the limit of detectability of AES. Exposures of the thermally annealed surface to oxygen to produce ~ 0.1 monolayer coverage, easily detected by AES, broadened the peak only 10—15%. These results indicate that the observed broadening cannot be due to systematic contamination induced by laser desorption from the chamber walls and windows.

In order to analyze these results more quantitatively, the observed peak width at $k_{\parallel} = 1.258$ Å^{-1} was measured as a function of laser-pulse energy density. Figure 3 shows the results of two distinct experiments. The lower curve was accumulated using a constant number of shots (50 in this case) from the laser for various pulse energies, while the upper curve was accumulated using a constant

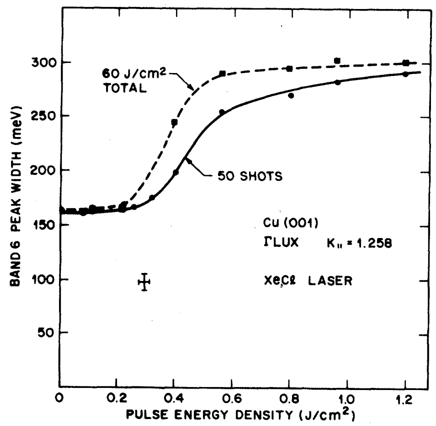

FIG. 3. Observed peak width as a function of laser pulse energy density. Lower curve: after 50 shots at the specified pulse energy. Upper curve: after 60 J/cm^2 integrated energy density.

total integrated energy density (60 J/cm^2). Both show three distinct regions. The first is a region (<0.3 J/cm^2 pulse energy) where the peak width is not affected significantly, indicating no surface degradation. Following this is a threshold region where the peak width increases and, presumably, defect formation caused by melting of the surface occurs. The width of this region probably has an experimental as well as a fundamental contribution. The fundamental contributions would include, for example, decreased defect production just below and just above threshold and an ill-defined melting temperature in the surface layers probed by ARP. The experimental contribution could result from spatial inhomogeneities produced by focusing the laser beam. Following the threshold region, the curves become relatively flat at higher pulse energies. The difference between the two curves in this final region is significant. To within the uncertainty of the experiment, the curve for constant total energy density is flat. Above threshold the electronic coherence length and the defect density in the surface layers are thus functions primarily of the integrated energy density and are not strongly affected by the pulse energy used. This result is due in part to the use of a surface sensitive probe. For higher pulse energies, the depth of the melted layer increases,[1,2] and presumably the total number of defects is larger. The defect density in the first few layers probed by electron spectroscopy apparently does not depend directly on the pulse energy well above threshold. If a different total energy density had been used, a curve with a similar shape but a different ultimate width in the third region would have been obtained.

There are several ways to portray this final result. The most relevant for our purposes is in terms of the electronic coherence length as a function of total energy dose for pulse energies well above threshold. In order to approximate this quantity, the various contributions to the observed width must be considered. In Fig. 3 a fundamental width of $\Gamma_0=160\pm5$ meV is observed following a thermal anneal. As explained in Sec. II, there are several contributions to Γ_0. The contribution from the final-state inverse lifetimes of the photohole and photoelectron states can be estimated from Eq. (9) to be ≤ 50 meV. There is also a contribution from the experimental energy resolution ($\Delta E \sim 25$ meV), and from the experimental and fundamental[12,14] momentum resolution ($\Delta E = \mathbf{v}_{\parallel}\cdot\Delta\mathbf{k}_{\parallel} \lesssim 150$ meV). The component of $\mathbf{v}_{\parallel}=\nabla_{\mathbf{k}}E$ along the $[\bar{1}10]$ axis is rather large in this case, a fact which makes both the experimental and fundamental momentum resolution quite important in determining the observed width. These various contributions convolute (not additively) to produce the observed width Γ_0. In order to extract rough value for the coherence length degradation following laser annealing, the observed width is artificially divided in two parts:

$$\Gamma=\Gamma_0+\mathbf{v}\cdot\Delta\mathbf{k}_0 \qquad (10)$$

Since only one component of $\mathbf{v}$ is significant (see Fig. 1), we actually will measure the projection of $\Delta\mathbf{k}_0$ along this axis, yielding a direct measure of the magnitude of the momentum broadening implied by Eq. (7). We define an electron coherence length in terms of the inverse of this broadening: $\bar{\lambda}=1/|\Delta\mathbf{k}_0|$. The addition in Eq. (10) implies a convolution as explained in Sec. II. Since the functional form of the second contribution is not well known, a value of $|\Delta\mathbf{k}_0|$ has been estimated using an average of values obtained assuming Lorentzian and Gaussian deconvolutions. The electron coherence length thus derived is plotted in Fig. 4. The error bars span the range between the Lorentzian and Gaussian limits, and are hence quite large near $E=0$, where the difference between Γ and Γ_0 is small. The approximations involved render this curve most useful as a semiquantitative guide to these results. The separation implied by Eq. (10) requires that this curve approach infinity at $E=0$. The coherence length is seen to drop quickly in the first 3–4 J/cm^2, and then to level off to a saturation coherence length of 30–40 Å at higher energy doses.

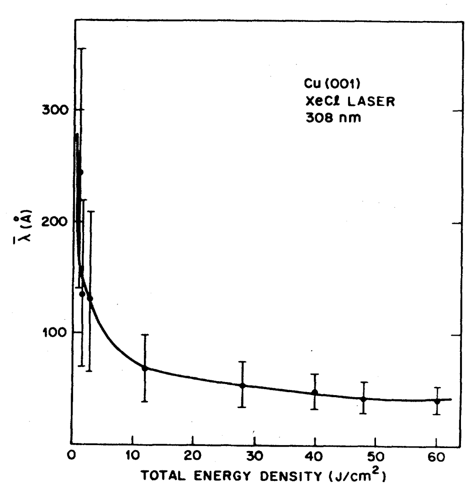

FIG. 4. Electron coherence length as a function of total energy density.

V. SUMMARY AND CONCLUSIONS

These results can be compared qualitatively with others in the literature. The largest total energies used in Fig. 4 are somewhat higher than those used in typical laser-annealing experiments. In this respect, the rapid decrease at low energies is more significant than the leveling off at higher energies. The scale of the vertical axis is significant; an electronic coherence length of ~ 100 Å is quite small by most standards. The mean separation of defects cannot be larger than this coherence length,[12] and is probably substantially shorter. A laser-annealed surface may not be appropriate for investigating defect-controlled surface processes. It is not clear how the defect density following PLA of copper will compare with that of other materials. Its high thermal conductivity is expected to lead to smaller thermal gradients and less mechanical stress during regrowth. On the other hand, the energy required to create a defect in a metallic system is smaller than in a covalent one, and the concentration of defects during the cooling cycle will consequently be higher in metals than in semiconductors.

In summary, angle-resolved photoemission has been used to study pulsed-laser-annealed Cu(001). The onset of melting was detected by the broadening of a sharp and rapidly dispersing peak in an energy distribution curve for laser pulse energy densities above ~ 0.3 J/cm^2. The source of the broadening was attributed to production of defects in the surface region, thereby reducing the electronic coherence length. The resulting coherence length was found to be nearly independent of pulse energy well above threshold, but to depend quite sensitively on the integrated energy density supplied to the surface.

[1] *Laser and Electron Beam Processing of Electronic Materials,* edited by G. L. Miller (Electrochemical Society, Princeton, N. J., 1979).

[2] *Laser and Electron Beam Processing of Materials,* edited by C. W. White and P. S. Percy (Academic, New York, 1980).

[3] D. M. Zehner, C. W. White, and G. Ownby, Appl. Phys. Lett. **36**, 56 (1980).

[4] P. L. Cowan and J. A. Golovchenko, J. Vac. Sci. Technol. **17**, 1197 (1980).

[5] Y. J. Chabal, J. E. Rowe, and D. A. Zwemer, Phys. Rev. Lett. **46**, 600 (1980).

[6] D. M. Zehner, C. W. White, P. Heimann, B. Reihl, F. J. Himpsel, and D. E. Eastman, Phys. Rev. B **24**, 4875 (1981).

[7] D. M. Zehner, C. W. White, P. Heimann, B. Reihl, F. J. Himpsel, and D. E. Eastman, Bull. Am. Phys. Soc. **26**, 226 (1981).

[8] J. M. Moison and M. Bensoussan, Surf. Sci. **126**, 294 (1983).

[9] L. Buene, J. M. Poate, D. C. Jacobson, C. W. Draper, and J. K. Hirvonen, Appl. Phys. Lett. **37**, 385 (1980).

[10] W. R. Wampler, D. M. Follstaedt, and P. S. Peercy, in *Laser and Electron Beam Solid Interactions and Materials Processing,* edited by J. F. Gibbons, L. D. Hess, and T. W. Sigmon (North-Holland, New York, 1981), p. 567.

[11] See *Laser and Electron Beam Processing of Materials,* Ref. 2, Sec. VII.

[12] J. Tersoff and S. D. Kevan, Phys. Rev. B **28**, 4267 (1983).

[13] S. D. Kevan, Phys. Rev. Lett. **50**, 526 (1983).

[14] S. D. Kevan, Phys. Rev. Lett. **50**, 526 (1983).

[15] Pierre Thiry, Ph.D. thesis, University of Paris, 1980.

[16] J. A. Knapp, F. J. Himpsel, and D. E. Eastman, Phys. Rev. B **19**, 4952 (1979).

[17] P. Thiry, D. Chandesris, J. Lecante, C. Guillot, R. Pinchaux, and Y. Petroff, Phys. Rev. Lett. **43**, 82 (1979).

[18] S. D. Kevan, Rev. Sci. Instrum. **54**, 1441 (1983).

[19] Lumonics, Inc., Model No. 860-3.